Polynomial decomposition method for ocular wavefront analysis

Damien Gatinel, Jacques Malet, Laurent Dumas

Research Article Vol. 35, No. 12 / December 2018 / Journal of the Optical Society of America A 2035

Journal of the Optical Society of America A
OPTICS, IMAGE SCIENCE, AND VISION

Polynomial decomposition method for ocular wavefront analysis

Damien Gatinel,[1,2,*] Jacques Malet,[1] and Laurent Dumas[2]

[1]Rothschild Foundation, Anterior Segment and Refractive Surgery Department, 25 rue Manin, Paris, France
[2]Laboratoire de Mathematiques de Versailles, UVSQ, CNRS, Universite Paris-Saclay, 78035 Versailles, France
*Corresponding author: gatinel@gmail.com

Received 2 August 2018; revised 8 October 2018; accepted 16 October 2018; posted 17 October 2018 (Doc. ID 341418); published 16 November 2018

Zernike circle polynomials are in widespread use for wavefront analysis because of their orthogonality over a circular pupil and their representation of balanced classical aberrations. However, some of the higher-order modes contain linear and quadratic terms. A new aberration series is proposed to better separate the low- versus higher-order aberration components. Because its higher-order modes are devoid of linear and quadratic terms, our new basis can be used to better fit the low- and higher-order components of the wavefront. This new basis may quantify the aberrations more accurately and provide clinicians with coefficient magnitudes which better underline the impact of clinically significant aberration modes.

https://doi.org/10.1364/JOSAA.35.002035

1. INTRODUCTION

Power series expansions have historically been used to describe and characterize optical system aberrations. Aberrometers measure all the eye's monochromatic aberrations and display the result in the form of an aberration map that describes the variation in optical path length from the source to retinal image through each point in the pupil. The wave aberration is expressed as a weighted sum of power series terms that are functions of the pupil coordinates. When the wavefront aberration is written as a series of its components, each mode can be regarded as a type of aberration. In ophthalmic optics, Zernike coefficients are usually specified using the standard nomenclature defined with reference to the standard coordinate system recommended by the Optical Society of America [1]. Zernike polynomials are orthogonal in a continuous fashion over the interior of a unit circle and, as many other functions, are convenient for serving as a complete basis [2–4]. They are usually expressed in polar coordinates, r and t, and are readily convertible to Cartesian coordinates. Any continuous wavefront f defined over a disk may be described as a sum of Zernike polynomials Z_n^m weighted by Zernike coefficients denoted $z_n^m(f)$. These polynomials are mutually orthogonal, making the variance of the sum of modes equal to the sum of the variances of each individual mode. Each mode of the Zernike polynomials minimizes the root mean squared (RMS) wavefront error to the order of that term. Each mode is constituted by the tensor product $R \otimes T$ of a polynomial $R(r)$ and a trigonometric function $T(t)$. They can be scaled so that non-zero-order modes have zero mean and unit variance. This common reference frame enables meaningful relative comparison between them and makes Zernike polynomials suitable for accurately describing wave aberrations as well as for data fitting.

The Zernike pyramid of aberration modes is organized by row (polynomial of order n) and by column (sine or cosine function of meridional frequency m) of the mathematical function Z_n^m that define the mode. The orthogonality of the modes of the same radial order n, which constitute the lines of the Zernike pyramid is ensured by the trigonometric function comprised within the tensor product since their azimuthal frequency differs. The orthogonality of the modes of the same azimuthal frequency m, which constitute the columns of the Zernike pyramid, is ensured by the orthogonality of the polynomials within the tensor products. These polynomials are generated using a Gram–Schmidt process. The lowest degree of the terms contained in the radial function of the Zernike mode is equal to the radial frequency of that mode. The value of this lowest degree corresponds to the valuation of the polynomial. The Gram–Schmidt process makes it orthogonal to each lower-order mode, and each mode contains the appropriate amount of each lower-order term. Hence, some polynomials of degree n may contain terms of lower degree than n. Whenever m differs from n, Zernike mode Z_n^m contains lower than n order terms. For example, when $m \leq 2$, higher-order ($n \geq 3$) modes contain tilt ($m = 1$) or defocus ($m = 0$ or $m = 2$) lower-order ($n \leq 2$) terms.

Part of the discrepancy between the second-order Zernike modes and the best subjective sphero-cylindrical error might be explained by the presence of second-order terms within higher-order modes [5,6]. In addition, the combination of the Zernike tilt modes does not reflect any possible tilt in the wavefront since tilt terms (r^1) are embedded in the $Z_3^{\pm 1}$ coma aberration modes. In ophthalmology, this mixing may have detrimental consequences on the understanding of the impact of higher-order aberrations (HOAs) on visual function. It has been shown that most of the visual impact of fourth-order Zernike aberrations can be attributed to the second-order terms within these polynomials [6].

In this paper, we propose new describing functions for the higher-order wavefront modes, which do not contain low (i.e., linear or quadratic) terms but maintain desirable mathematical properties, such as orthogonality and normality.

Different decomposition schemes are examined which include azimuthal and commonly used Zernike expansions, as well as a newly proposed series expansion, which has several advantages over the Zernike scheme. This alternative series expansion leads to a new decomposition scheme for ophthalmic work, where the low- and higher-order aberration components of the wavefront may be better separated and analyzed.

2. LOW-DEGREE HIGH-DEGREE DECOMPOSITION AND A SUITABLE BASIS

A. Mathematical Treatment of Wavefronts

On a mathematically simplified viewpoint, the normalized pupil is identified with the $\mathbf{R}^2$ unit disc $\mathbf{D}$:

$$\mathbf{D} \coloneqq \{(x,y) \in \mathbf{R}^2; x^2 + y^2 \leq 1\}, \tag{1}$$

$$\mathbf{D} = \{(r\cos(t), r\sin(t)); 0 \leq r \leq 1, -\pi \leq t \leq +\pi\}. \tag{2}$$

The eye wavefront will then be seen as a real valued function f defined on $\mathbf{D}$:

$$f: \begin{cases} \mathbf{D} \to \mathbf{R} \\ (x,y) \mapsto f(x,y) \end{cases}. \tag{3}$$

This function is assumed to be polynomial, without any loss of generality, since linear combinations of $x^k y^\ell$ monomials provide arbitrarily close approximations of any continuous function on $\mathbf{D}$. In clinical applications, the total degree of this polynomial function rarely exceeds 6.

One then defines the inner (or scalar) product of two wavefronts f and g as

$$\langle f,g\rangle_{\mathbf{D}} \coloneqq \frac{1}{\pi}\iint_{\mathrm{D}} f(x,y)g(x,y)\mathrm{d}x\mathrm{d}y. \tag{4}$$

This inner product provides the space of polynomial wavefronts with a geometrical structure, and allows us to consider wavefronts as vectors in an Euclidian space. It also provides the means of defining orthogonality between wavefronts (with zero inner product) and the distance between two wavefronts as

$$d(f,g) \coloneqq \left(\frac{1}{\pi}\iint_{\mathbf{D}} (f(x,y) - g(x,y))^2 \mathrm{d}x\mathrm{d}y\right)^{1/2}. \tag{5}$$

The classical RMS is the distance from a wavefront to its average:

$$p_0(f) \coloneqq \frac{1}{\pi}\iint_{\mathbf{D}} f(x,y)\mathrm{d}x\mathrm{d}y \text{ (piston)},$$

$$\mathrm{RMS} = d(f, p_0(f)) = \left(\frac{1}{\pi}\iint_{\mathbf{D}} (f(x,y) - p_0(f))^2 \mathrm{d}x\mathrm{d}y\right)^{1/2}.$$

B. Azimuthal Expansion and Low-Degree High-Degree Decomposition

Every polynomial wavefront has a Taylor expansion, given by

$$f = \sum_{n\geq 0}\sum_{m\in I_n} x_n^m(f) X_n^m, \tag{6}$$

where

$$\begin{cases} X_n^m \coloneqq (x,y) \mapsto x^{\frac{n+m}{2}} y^{\frac{n-m}{2}} \\ x_n^m(f) \coloneqq \frac{1}{n!}\frac{\partial^n f}{\partial x^{\frac{n+m}{2}} \partial y^{\frac{n-m}{2}}}(0,0) \end{cases}.$$

Using a Fourier expansion of degree homogeneous terms in Eq. (6), one gets a new expansion of f, called its azimuthal expansion.

Sorted by radial degree n, and for a given degree in increasing order of azimuthal frequency m, the azimuthal expansion of f can be written

$$f = \sum_{n\geq 0}\left(\sum_{m\in I_n} a_n^m(f) A_n^m\right), \tag{7}$$

or, expressed in trigonometric form,

$$f(r\cos(t), r\sin(t)) = \sum_{n\geq 0}\left(\sum_{m\in I_n} a_n^m(f) R_{(n)}(r) T_m(t)\right), \tag{8}$$

where $R_{(n)}: r \mapsto \sqrt{n+1}\, r^n$ are normed monomials.

Azimuthal polynomial functions A_n^m with different azimuthal frequencies m are orthogonal, but the whole azimuthal basis is not orthonormal.

The main advantage of azimuthal basis relies in the degree separation they allow. Whereas Zernike expansion Eq. (15) mixes low-degree and higher-degree monomials, expansions Eqs. (6) and (7) allow a clear-cut separation between them.

Let $\mathcal{L}_{\mathbf{D}}$ be the vector space of low-degree (≤ 2) wavefronts:

$$\mathcal{L}_{\mathbf{D}} \coloneqq \mathrm{span}\{A_n^m; n \leq 2, m \in I_n\}, \tag{9}$$

where

$$\begin{aligned} A_0^0 &= 1, \\ A_1^{-1} &= 2r\sin(t) = 2y, \\ A_1^{+1} &= 2r\cos(t) = 2x, \\ A_2^{-2} &= r^2\sqrt{6}\sin(2t) = 2\sqrt{6}xy, \\ A_2^0 &= \sqrt{3}r^2 = \sqrt{3}(x^2+y^2), \\ A_2^{+2} &= r^2\sqrt{6}\cos(2t) = \sqrt{6}(x^2-y^2). \end{aligned}$$

The vector space $\mathcal{P}_{\mathbf{D}}$ of all polynomial wavefronts admits a direct sum decomposition,

$$\mathcal{P}_{\mathbf{D}} = \mathcal{L}_{\mathbf{D}} \oplus \mathcal{H}_{\mathbf{D}}, \tag{10}$$

where $\mathcal{H}_{\mathbf{D}}$ is the vector space of wavefronts with no low-degree monomial:

$$\mathcal{H}_{\mathbf{D}} := \mathrm{span}\{A_n^m; n \geq 3, m \in I_n\}. \tag{11}$$

For every polynomial wavefront f there is a unique couple (f_ℓ, f_h) of polynomial wavefronts, the former in $\mathcal{L}_{\mathbf{D}}$, the latter in $\mathcal{H}_{\mathbf{D}}$, such that

$$f = f_\ell + f_h. \tag{12}$$

Low-degree and higher-degree components f_ℓ and f_h are easily derived from azimuthal expansion Eq. (7):

$$f_\ell = \sum_{n=0}^{2} \left(\sum_{m \in I_n} a_n^m(f) A_n^m \right), \tag{13}$$

$$f_h = \sum_{n \geq 3} \left(\sum_{m \in I_n} a_n^m(f) A_n^m \right). \tag{14}$$

Decomposition Eq. (12) will be called the low-degree high-degree (LDHD) decomposition of f.

C. Zernike Expansion

Sorted by radial degree n, and for a given degree in increasing order of azimuthal frequency m, the well-known Zernike expansion of a wavefront f is

$$f = \sum_{n \geq 0} \left(\sum_{m \in I_n} z_n^m(f) Z_n^m \right), \tag{15}$$

or, expressed in its trigonometric form,

$$f(r\cos(t), r\sin(t)) = \sum_{n \geq 0} \left(\sum_{m \in I_n} z_n^m(f) R_n^m(r) T_m(t) \right), \tag{16}$$

where

$$\begin{cases} I_n := \{-n, -n+2, \ldots, +n-2, +n\} \\ T_m(t) := \begin{cases} \sqrt{2}\sin(-mt) & \text{si } m < 0 \\ 1 & \text{si } m = 0 \\ \sqrt{2}\cos(mt) & \text{si } m > 0 \end{cases} \\ R_n^m(r) := \sqrt{n+1} \sum\limits_{0 \leq k \leq \frac{n-|m|}{2}} (-1)^k \frac{(n-k)!}{k!\left(\frac{n-m}{2}-k\right)!\left(\frac{n+m}{2}-k\right)!} r^{n-2k} \end{cases}.$$

For example,

$$\begin{aligned} R_0^0(r) &= 1, \\ R_1^{-1}(r) &= R_1^1(r) = \sqrt{2}r, \\ R_2^{-2}(r) &= R_2^2(r) = \sqrt{3}\, r^2, \\ R_2^0(r) &= \sqrt{3}(2r^2 - 1), \\ R_3^{-3}(r) &= R_3^3(r) = 2r^3, \\ R_3^1(r) &= R_3^{-1}(r) = 2(3r^3 - 2r), \\ R_4^{-4}(r) &= R_4^4(r) = \sqrt{5}\, r^4, \\ R_4^{-2}(r) &= R_4^2(r) = \sqrt{5}(4r^4 - 3r^2), \\ R_4^0(r) &= \sqrt{5}(6r^4 - 6r^2 + 1). \end{aligned}$$

Azimuthal functions T_m form an orthonormal set with respect to the inner product:

$$(U, V) \mapsto \langle U, V \rangle_{\mathrm{azi}} := \frac{1}{2\pi} \int_{-\pi}^{+\pi} U(t) V(t) \mathrm{d}t. \tag{17}$$

Radial polynomial functions R_n^m form an orthonormal set with respect to the inner product:

$$(R, S) \mapsto \langle R, S \rangle_{\mathrm{rad}} := 2 \int_0^1 R(r) S(r) r \mathrm{d}r. \tag{18}$$

Therefore, bivariate functions

$$Z_n^m = R_n^m \otimes T_m := (r, t) \mapsto R_n^m(r) T_m(t)$$

form an orthonormal set with respect to the inner product given by Eq. (4). They are classically called *Zernike polynomials*, whereas numerical coefficients z_n^m in Eq. (15) are called the *Zernike coefficients* of wavefront f.

D. New Basis for High-Degree Wavefronts

Starting with the azimuthal basis $(A_n^m)_{n \geq 3, m \in I_n}$ of $\mathcal{H}_{\mathbf{D}}$ and using Gram–Schmidt procedure, we have derived an orthonormal basis $(G_n^m)_{n \geq 3, m \in I_n}$ of $\mathcal{H}_{\mathbf{D}}$.

For all $n \geq 3$ and $m \in I_n$,

$$G_n^m := \begin{cases} R_n^{3+\mathbf{1}_{2\mathbf{N}}(n)} \otimes T_m & \text{if } |m| \leq 2 \\ R_n^m \otimes T_m & \text{otherwise} \end{cases}, \tag{19}$$

where $\mathbf{1}_{2\mathbf{N}}(n) = 1$ if n is even, 0 if n is odd.

Thus, polynomial wavefronts G_n^m ($n \geq 3$ and $m \in I_n$) given by Eq. (19) form an orthonormal basis of $\mathcal{H}_{\mathbf{D}}$ with respect to the inner product Eq. (4). Polynomial wavefronts Z_n^m ($n \geq 3$ and $m \in I_n$) still form an orthonormal family but are not low-order free: whenever it differs from G_n^m, polynomial wavefront Z_n^m does not belong to $\mathcal{H}_{\mathbf{D}}$:

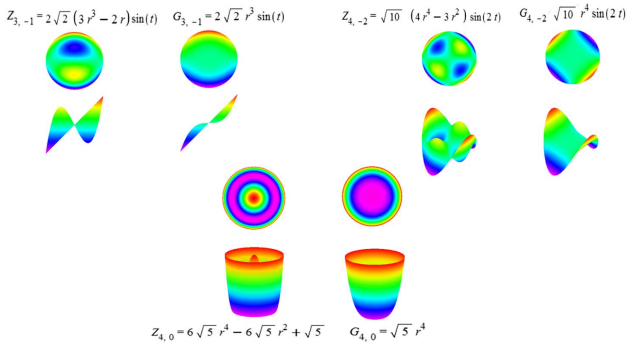

Fig. 1. Visualization of the differences between the Zernike and new LDHD modes of clinical importance.

$$G_3^{-3} = Z_3^{-3} = 2\sqrt{2}r^3 \sin(3t), \quad G_3^{-1} = 2\sqrt{2}r^3 \sin(t), \quad Z_3^{-1} = 2\sqrt{2}(3r^3 - 2r)\sin(t),$$
$$G_3^{+1} = 2\sqrt{2}r^3 \cos(t), \quad Z_3^{+1} = 2\sqrt{2}(3r^3 - 2r)\cos(t), \quad G_3^{+3} = Z_3^{33} = 2\sqrt{2}r^3 \cos(3t),$$
$$G_4^{-4} = Z_4^{-4} = \sqrt{10}r^4 \sin(4t), \quad G_4^{-2} = \sqrt{10}r^4 \sin(2t), \quad Z_4^{-2} = \sqrt{10}(4r^4 - 3r^2)\sin(2t), \quad G_4^0 = \sqrt{5}r^4,$$
$$Z_4^0 = \sqrt{5}(6r^4 - 6r^2 + 1), \quad G_4^2 = \sqrt{10}r^4 \cos(2t), \quad Z_4^{-2} = \sqrt{10}(4r^4 - 3r^2)\sin(2t),$$
$$G_4^{+4} = Z_4^{+4} = \sqrt{10}r^4 \cos(4t), \quad G_5^{-5} = Z_5^{-5} = 2\sqrt{3}r^5 \sin(5t), \quad G_5^{-3} = Z_5^{-3} = 2\sqrt{3}(5r^5 - 4r^3)\sin(3t),$$
$$G_5^{-1} = 2\sqrt{3}(5r^5 - 4r^3)\sin(t), \quad Z_5^{-1} = 2\sqrt{3}(10r^5 - 12r^3 + 3r)\sin(t), \quad G_5^{+1} = 2\sqrt{3}(5r^5 - 4r^3)\cos(t),$$
$$Z_5^{+1} = 2\sqrt{3}(10r^5 - 12r^3 + 3r)\cos(t), \quad G_5^{+3} = Z_5^{+3} = 2\sqrt{3}(5r^5 - 4r^3)\cos(3t), \quad G_5^{+5} = Z_5^{+5} = 2\sqrt{3}r^5 \cos(5t),$$
$$G_6^{-6} = Z_6^{-6} = \sqrt{14}r^6 \sin(6t), \quad G_6^{-4} = Z_6^{-4} = \sqrt{14}(6r^6 - 5r^4)\sin(4t), \quad G_6^{-2} = \sqrt{14}(6r^6 - 5r^4)\sin(2t),$$
$$Z_6^{-2} = \sqrt{14}(15r^6 - 20r^4 + 6r^2)\sin(2t), \quad G_6^0 = \sqrt{7}(6r^6 - 5r^4), \quad Z_6^0 = \sqrt{7}(20r^6 - 30r^4 + 12r^2 - 1),$$
$$G_6^{+2} = \sqrt{14}(6r^6 - 5r^4)\cos(2t), \quad Z_6^{+2} = \sqrt{14}(15r^6 - 20r^4 + 6r^2)\cos(2t), \quad G_6^{+4} = Z_6^{+4} = \sqrt{14}(6r^6 - 5r^4)\cos(4t),$$
$$G_6^{+6} = Z_6^{+6} = 2\sqrt{14}r^6 \cos(6t), \quad G_7^{-7} = Z_7^{-7} = 4r^7 \sin(7t), \quad G_7^{-5} = Z_5^{-5} = 4(7r^7 - 6r^5)\sin(5t),$$
$$G_7^{-3} = Z_7^{-3} = 4(21r^7 - 30r^5 + 10r^3)\sin(3t), \quad G_7^{-1} = 4(21r^7 - 30r^5 + 10r^3)\sin(t),$$
$$Z_7^{-1} = 4(35r^7 - 60r^5 + 30r^3 - 4r)\sin(t), \quad G_7^{+1} = 4(21r^7 - 30r^5 + 10r^3)\cos(t), \quad Z_7^{+1} = 4(35r^7 - 60r^5 + 30r^3 - 4r)\cos(t),$$
$$G_7^{+3} = Z_7^{+3} = 4(21r^7 - 30r^5 + 10r^3)\cos(3t), \quad G_7^{+5} = Z_5^{+5} = 4(7r^7 - 6r^5)\cos(5t), \quad G_7^{+7} = Z_7^{+7} = 4r^7 \cos(7t).$$

Figure 1 allows visualization of the differences between modes of clinical importance (including coma $Z_3^{\pm 1}$, spherical aberration Z_4^0, and secondary astigmatism $Z_4^{\pm 2}$).

E. New Expansion and Coefficients

Low-degree Zernike polynomials $Z_n^m (n \leq 2)$ provide a basis for $\mathcal{L}_\mathbf{D}$. Concatenating this basis with the new basis for $\mathcal{H}_\mathbf{D}$, one gets a complete set of modes, i.e., a basis of $\mathcal{P}_\mathbf{D}$.

The corresponding wavefront error envelopes of these modes is represented in Fig. 2.

Using this basis of $\mathcal{P}_\mathbf{D}$, we get the following new expansion of any polynomial wavefront f, which we will call its new expansion:

$$\begin{aligned} f &= f_\ell + f_h \\ &= \sum_{n=0}^{2}\left(\sum_{m\in I_n} g_n^m(f) Z_n^m\right) + \sum_{n\geq 3}\left(\sum_{m\in I_n} g_n^m(f) G_n^m\right), \end{aligned} \tag{20}$$

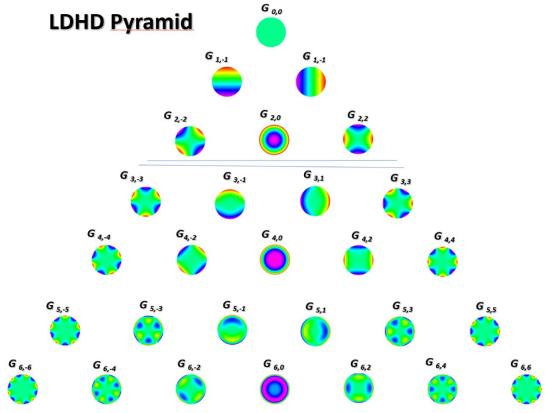

Fig. 2. Pyramid of the new expansion mode envelopes.

where

$$\begin{cases} g_n^m(f) = \langle f_\ell, Z_n^m\rangle_\mathbf{D} & \text{if } n \leq 2 \\ g_n^m(f) = \langle f_h, G_n^m\rangle_\mathbf{D} & \text{if } n \geq 3 \end{cases},$$

since $(Z_n^m)_{n\leq 2, m\in I_n}$ is an orthonormal basis of $\mathcal{L}_\mathbf{D}$ and $(G_n^m)_{n\geq 3, m\in I_n}$ is an orthonormal basis of $\mathcal{H}_\mathbf{D}$.

Low-degree and higher-degree components f_ℓ and f_h do not immediately follow from Zernike expansion Eq. (15), but they are easily derived from azimuthal expansion Eq. (7).

In order to get f_l component in LDHD decomposition Eq. (12) from Zernike expansion, one has to collect low-order terms.

Let $c_{n+2p}^m(n)$ be the nth degree coefficient in radial polynomial function R_{n+2p}^m.

For every integer $p \geq 0$,

$$c_{n+2p}^m(n) = \sqrt{n+2p+1}\,\frac{(-1)^p(n+p)!}{p!\left(\frac{n-m}{2}\right)!\left(\frac{n+m}{2}\right)!}, \tag{21}$$

since

$$R_{n+2p}^m(r) = \sqrt{n+2p+1}\sum_{0\leq k\leq \frac{n+2p-|m|}{2}} (-1)^k \times \frac{(n+2p-k)!}{k!\left(\frac{n+2p-m}{2}-k\right)!\left(\frac{n+2p+m}{2}-k\right)!}\, r^{n+2p-2k}.$$

Cumulating terms of the same degree, we get

$$a_n^m(f) = \sum_{p\geq 0} z_{n+2p}^m(f) c_{n+2p}^m(n). \tag{22}$$

Henceforth, new low-order coefficients can be obtained through orthogonal projection on linear subspace $\mathcal{L}_\mathbf{D}$,

$$f_\ell = \sum_{n=0}^{2}\left(\sum_{m\in I_n}\left(\sum_{p\geq 0} z_{n+2p}^m(f)c_{n+2p}^m(n)\right)\right)A_n^m$$
$$= \sum_{n=0}^{2}\left(\sum_{m\in I_n} g_n^m(f)Z_n^m\right), \quad (23)$$

and new higher-order coefficients can be obtained through orthogonal projection on linear subspace $\mathcal{H}_{\mathbf{D}}$,

$$f_h = f - f_\ell = \sum_{n\geq 3}\left(\sum_{m\in I_n} g_n^m(f)G_n^m\right). \quad (24)$$

Using either Zernike $(Z_n^m)_{0\leq n\leq N}$ or $(Z_n^m)_{n\leq 2}$ and $(G_n^m)_{3\leq n\leq N}$ functions to fit an arbitrary wavefront shape would produce the same polynomial function f, since both sets of functions provide a basis of the same vector space. This space is the set of all polynomial wavefronts with a maximal chosen degree (e.g., $N = 6$). Therefore, the residual errors would be exactly the same in both methods.

3. SPATIAL REPRESENTATIONS

The purpose of this section is to provide geometrical representations of Zernike and GM expansions, in order to visualize their differences. These representations must be faithful to the Euclidean geometry of wavefronts defined by the inner product Eq. (4).

A. Pseudo-Variances and Pseudo-RMS

In order to compare clinically relevant lower-order terms, we decided to remove piston and tilt coefficients and work with "centered and aligned" wavefronts.

Centering and aligning a wavefront f provides a zero mean zero tilt wavefront ($z_0^0(f^*) = 0$, $z_1^{-1}(f^*) = 0$, $z_1^{+1}(f^*) = 0$) f^* given by Eq. (25):

$$f^* = f - z_0^0(f)Z_0^0 - z_1^{-1}(f)Z_1^{-1} - z_1^{+1}(f)Z_1^{+1}$$
$$= \sum_{n\geq 2}\left(\sum_{m\in I_n} z_n^m(f)Z_n^m\right). \quad (25)$$

We then define the pseudo-variance and pseudo-RMS of f as the variance and RMS of f^* [Eqs. (26) and (27)]:

$$V^*(f) = \|f^*\|_{\mathbf{D}}^2 = \frac{1}{\pi}\iint_{\mathbf{D}} (f^*(x,y))^2 \mathrm{d}x\mathrm{d}y$$
$$= \sum_{n\geq 2}\left(\sum_{m\in I_n}(z_n^m(f))^2\right), \quad (26)$$

$$\mathrm{RMS}^*(f) = \sqrt{V^*(f)}. \quad (27)$$

B. Geometry of Wavefront Functions

Geometrically speaking, wavefront pseudo-RMS is tantamount to the vector length:

$$\|f^*\|_{\mathbf{D}} = \sqrt{V^*(f)}. \quad (28)$$

Likewise, the "angle" of two wavefronts may be defined from their "pseudo-covariance,"

$$C^*(f,g) = \langle f^*, g^*\rangle_{\mathbf{D}} = \frac{1}{\pi}\iint_{\mathbf{D}} f^*(x,y)g^*(x,y)\mathrm{d}x\mathrm{d}y$$
$$= \sum_{n\geq 2}\left(\sum_{m\in I_n} z_n^m(f)z_n^m(g)\right), \quad (29)$$

through Eq. (30):

$$\mathrm{Angle}^*(f,g) = \mathrm{ArcCos}\left(\frac{C^*(f,g)}{\|f^*\|_{\mathbf{D}}\|g^*\|_{\mathbf{D}}}\right). \quad (30)$$

Accordingly, the whole geometrical configuration of several wavefronts may be derived from the Gram matrix of their pseudo-variances and covariances.

Gram matrix $G(f)$ in Eq. (31) summarizes the geometrical configuration of Zernike and new LDHD decompositions:

$$G(f) = \begin{pmatrix} V^*(f_{z\ell}) & 0 & C^*(f_{z\ell}, f_\ell) & C^*(f_{z\ell}, f_h) \\ 0 & V^*(f_{zh}) & 0 & C^*(f_{zh}, f_h) \\ C^*(f_\ell, f_{z\ell}) & 0 & V^*(f_\ell) & C^*(f_\ell, f_h) \\ C^*(f_h, f_{z\ell}) & C^*(f_h, f_{zh}) & C^*(f_h, f_\ell) & V^*(f_h) \end{pmatrix}, \quad (31)$$

where

$$\begin{cases} f_{z\ell} = \sum_{n=0}^{2}\left(\sum_{m\in I_n} z_n^m(f)Z_n^m\right) \\ f_{zh} = \sum_{n\geq 3}\left(\sum_{m\in I_n} z_n^m(f)Z_n^m\right) \\ f_\ell = \sum_{n=0}^{2}\left(\sum_{m\in I_n} g_n^m(f)Z_n^m\right) \\ f_h = \sum_{n\geq 3}\left(\sum_{m\in I_n} g_n^m(f)G_n^m\right) \end{cases}.$$

C. Four Spatial Representations

Higher than 3D representations being impossible, we chose the most significant spatial representations to describe the geometrical structure of LDHD decompositions.

1. Zernike versus New LD Expansion

Low-degree $f_{z\ell}^*$ and f_ℓ^* expansions in orthonormal basis $(Z_2^{-2}, Z_2^0, Z_2^{+2})$ allow the following three-dimensional representation of low-degree components $f_{z\ell}$ and f_ℓ:

$$f_\ell^* = \langle f_\ell^*, Z_2^{-2}\rangle_{\mathbf{D}} Z_2^{-2} + \langle f_\ell^*, Z_2^0\rangle_{\mathbf{D}} Z_2^0 + \langle f_\ell^*, Z_2^{+2}\rangle_{\mathbf{D}} Z_2^{+2}, \quad (32)$$

$$f_{z\ell}^* = \langle f_{z\ell}^*, Z_2^{-2}\rangle_{\mathbf{D}} Z_2^{-2} + \langle f_{z\ell}^*, Z_2^0\rangle_{\mathbf{D}} Z_2^0 + \langle f_{z\ell}^*, Z_2^{+2}\rangle_{\mathbf{D}} Z_2^{+2}. \quad (33)$$

2. Zernike versus New LDHD Decomposition

Expanding zero mean zero tilt LDHD decompositions

$$f^* = f_{z\ell}^* + f_{zh}^* = f_\ell^* + f_h^*$$

in orthonormal basis

$$\begin{cases} U_{f,1} = \frac{1}{\|f^*_{z\ell}\|_{\mathbf{D}}} f^*_{z\ell} \\ U_{f,2} = \frac{1}{\|f^*_{zh}\|_{\mathbf{D}}} f^*_{zh} \\ U_{f,3} = \frac{1}{\|f^*_{z\ell}\|_{\mathbf{D}}} f^*_{z\ell} \times \frac{1}{\|f^*_{zh}\|_{\mathbf{D}}} f^*_{zh} \end{cases}$$

allows the following three-dimensional representation of Zernike and new LDHD decompositions:

$$f^*_{z\ell} = \|f^*_{z\ell}\|_{\mathbf{D}} U_{f,1},$$
$$f^*_{zh} = \|f^*_{zh}\|_{\mathbf{D}} U_{f,2},$$
$$f^*_{\ell} = \langle f^*_{\ell}, U_{f,1}\rangle_{\mathbf{D}} U_{f,1} + \langle f^*_{\ell}, U_{f,3}\rangle_{\mathbf{D}} U_{f,3},$$
$$f^*_{h} = \langle f^*_{h}, U_{f,1}\rangle_{\mathbf{D}} U_{f,1} + \langle f^*_{h}, U_{f,2}\rangle_{\mathbf{D}} U_{f,2} + \langle f^*_{h}, U_{f,3}\rangle_{\mathbf{D}} U_{f,3}.$$

3. Zernike HD Expansion

Zernike higher-degree component f^*_{zh} may be expanded as

$$f^*_{zh} = f^*_{zh3} + f^*_{zh4} + f^*_{zh56}, \tag{34}$$

where

$$\begin{cases} f^*_{zh3} = \sum_{m\in I_3} z^m_3(f) Z^m_3 \\ f^*_{zh4} = \sum_{m\in I_4} z^m_4(f) Z^m_4 \\ f^*_{zh56} = \sum_{n\geq 5} \left(\sum_{m\in I_n} z^m_n(f) Z^m_n \right) \end{cases}.$$

Expanding f^*_{zh} in orthonormal basis

$$\begin{cases} U_{fzh,1} = \frac{1}{\|f^*_{zh3}\|_{\mathbf{D}}} f^*_{zh3} \\ U_{fzh,2} = \frac{1}{\|f^*_{zh4}\|_{\mathbf{D}}} f^*_{zh4} \\ U_{fzh,3} = \frac{1}{\|f^*_{zh56}\|_{\mathbf{D}}} f^*_{zh56} \end{cases}$$

allows the following three-dimensional representation of Zernike high-degree component f_{zh}:

$$f^*_{zh} = \|f^*_{zh3}\|_{\mathbf{D}} U_{fzh,1} + \|f^*_{zh4}\|_{\mathbf{D}} U_{fzh,2} + \|f^*_{zh56}\|_{\mathbf{D}} U_{fzh,3}.$$

4. New HD Expansion

High-degree component f^*_h may be expanded as

$$f^*_h = f^*_{h3} + f^*_{h4} + f^*_{h56}, \tag{35}$$

where

$$\begin{cases} f^*_{h3} = \sum_{m\in I_3} g^m_3(f) G^m_3 \\ f^*_{h4} = \sum_{m\in I_4} g^m_4(f) G^m_4 \\ f^*_{h56} = \sum_{n\geq 5} \left(\sum_{m\in I_n} g^m_n(f) G^m_n \right) \end{cases}.$$

Expanding f^*_h in orthonormal basis

$$\begin{cases} U_{fh,1} = \frac{1}{\|f^*_{h3}\|_{\mathbf{D}}} f^*_{h3} \\ U_{fh,2} = \frac{1}{\|f^*_{h4}\|_{\mathbf{D}}} f^*_{h4} \\ U_{fh,3} = \frac{1}{\|f^*_{h56}\|_{\mathbf{D}}} f^*_{h56} \end{cases}$$

allows the following three-dimensional representation of Zernike high-degree component f_h:

$$f^*_h = \|f^*_{h3}\|_{\mathbf{D}} U_{fh,1} + \|f^*_{h4}\|_{\mathbf{D}} U_{fh,2} + \|f^*_{h56}\|_{\mathbf{D}} U_{fh,3}. \tag{36}$$

In all these 3D representations, note that the 3D orthonormal basis will not be shown.

4. THEORETICAL EXAMPLES

Figure 3 shows an artificial set of third-order LDHD coefficients of a wavefront aberration over a circular pupil, each loaded with 1 μm, and the corresponding Zernike expansion. In addition to the introduction of Zernike tilt, the value of the Zernike coma coefficient is one third of its corresponding LDHD mode. The trefoil modes coefficients are not affected, since their analytical expressions do not differ between the two decompositions.

Figure 4 shows an artificial set of third-order Zernike coefficients of a wavefront aberration over a circular pupil, each loaded with 1 μm, and the corresponding LDHD expansion. This conversion reveals the tilt contained in the coma modes of the Zernike classification. The value of the coma coefficient is multiplied by 3 in the LDHD classification. The trefoil modes coefficients are not affected, since their analytical expressions do not differ between the two decompositions.

Figure 5 shows an artificial set of fourth-order LDHD coefficients of a wavefront aberration over a circular pupil, each loaded with 1 μm, and the corresponding Zernike expansion.

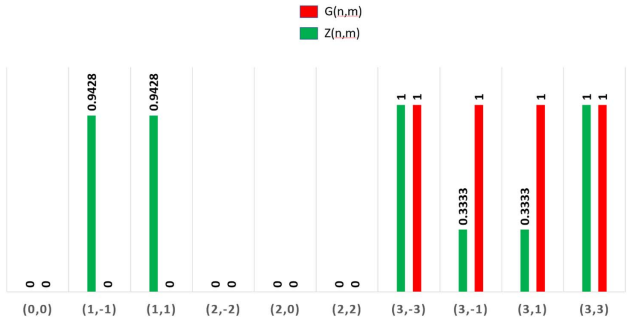

Fig. 3. Visualization of the differences between the Zernike and new third-order coefficients.

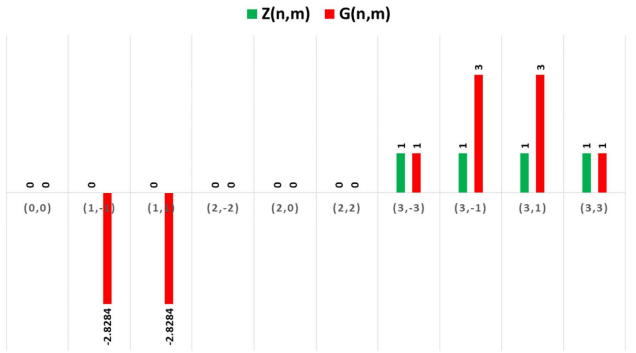

Fig. 4. Visualization of the differences between the new LDHD and Zernike third-order coefficients.

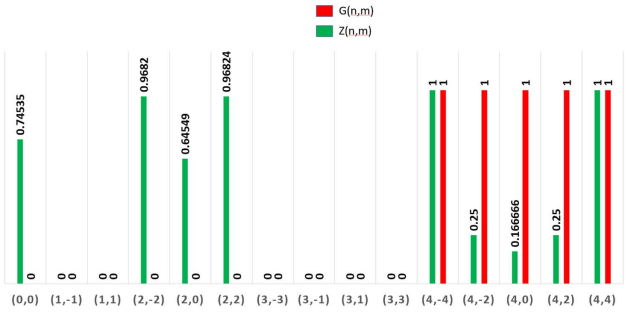

Fig. 5. Visualization of the differences between the Zernike and new fourth-order coefficients.

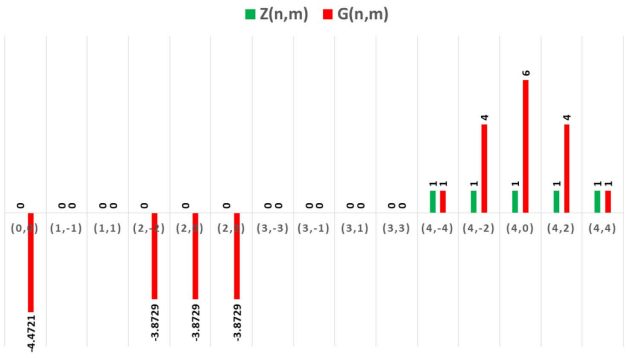

Fig. 6. Visualization of the differences between the new LDHD and Zernike fourth-order coefficients.

In addition to the introduction of piston, Zernike defocus and astigmatism modes non-null coefficients, the value of the Zernike spherical aberration and secondary astigmatism coefficients are one fourth and one sixth of that of their corresponding LDHD modes. The quadrafoil modes coefficients are not affected.

Figure 6 shows an artificial set of fourth-order Zernike coefficients of a wavefront aberration over a circular pupil, each loaded with 1 μm, and the corresponding LDHD expansion. This conversion reveals the piston and defocus contained in the fourth-order spherical aberration mode of the Zernike classification, and the second-order astigmatism contained in the fourth-order astigmatism modes of the Zernike classification. The value of the LDHD spherical aberration coefficient is multiplied by 6, and that of the secondary astigmatism by 4. The quadrafoil modes coefficients are not affected, since their analytical expressions do not differ between the two decompositions.

5. CLINICAL EXAMPLES

The Zernike coefficients were obtained from automated retinoscopy with an infrared light beam (808 nm wavelength) and aberrometry measurement using the OPD-scan III instrument (Nidek, Gammagori, Japan) on a 6 mm pupil (natural dilatation in mesopic conditions). The coefficients of the LDHD decomposition were obtained from the procedure described in subsection 2.D. The spatial representations were generated using the method described in Section 3.

A. Myopic Eye

Figure 7 enables comparison between the Zernike and LDHD decompositions of the wavefront of a myopic eye with a 6 mm pupil. The value of the tilt coefficients $g_1^{\pm 1}$ is negligible, which suggests that after the collection of all the tilt terms in r^1 from the total wavefront analytical expression, the total tilt of the wavefront has vanished. The value of the defocus and astigmatism terms are not significantly different between the two decompositions. The magnitude and signs of the coefficients weighting the third- and fifth-order coma and fourth- and sixth-order spherical aberration differ slightly between the two expansions.

The spatial representation of the LD expansion (see Fig. 8) reflects the proximity in the magnitude of the low-order modes coefficients. The lack of orthogonality between the low f_l^* and the high f_h^* wavefront components of the LDHD expansion is evidenced on the Zernike versus new HD spatial representations.

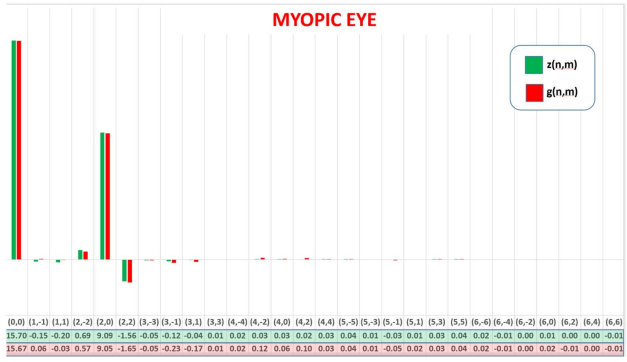

Fig. 7. Comparison between the Zernike and new expansion coefficients of a myopic eye.

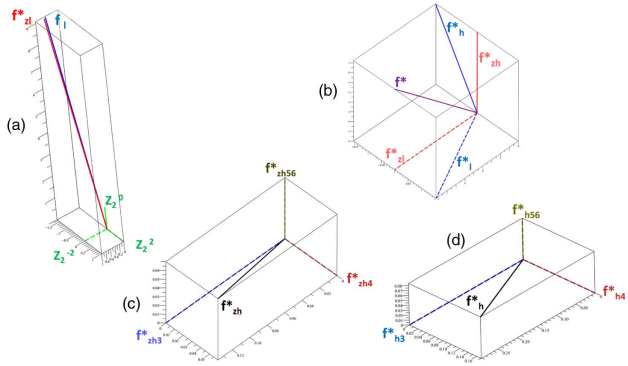

Fig. 8. Geometrical representations of the Zernike and GM expansions: (a) comparison of $f_{z\ell}$ and f_ℓ; (b) comparison of the Zernike versus LDHD split between low ($f_{z\ell}$ versus f_ℓ) and high (f_{zh} versus f_h) components; (c),(d) comparison between the Zernike HD versus new HD expansion.

B. Eye with Keratoconus

The comparison between the Zernike and LDHD decompositions reveals the presence of large differences between the value of the low-degree astigmatism coefficient ($g_2^{-2} = 4.6$ μm, $z_2^{-2} = 1.46$ μm) (Fig. 9). This difference is explained by the presence of low-order astigmatism terms within the secondary astigmatism Zernike modes $Z_4^{\pm 2}$. Because the $G_4^{\pm 2}$ modes of the LDHD classification are free of these terms, they are all collected in the low-order wavefront component and this results in an increase in the magnitude of the total low-order astigmatism. The magnitude of the tilt coefficients in the Zernike decomposition mostly results from the necessity to compensate for the tilt terms present in the coma modes $Z_3^{\pm 1}$.

The spatial representation of the LD expansion (Fig. 10) reflects the difference in the magnitude of the low-order modes coefficients. The lack of orthogonality between the low f_ℓ^* and the high f_h^* wavefront components of the LDHD expansion is evidenced on the Zernike versus new HD spatial representation. While the magnitude of all the third-order modes coefficients (f_{zh3}^*) seem to predominate in the Zernike HD component (f_{zh}^*), the repartition between the third- and fourth-order aberration compartments is more balanced in the new HD expansion f_h^*.

C. Eye Operated with LASIK for High Myopia

Figure 11 represents a histogram of the coefficients obtained from the wavefront reconstruction between the Zernike and LDHD polynomial basis. The patient is emmetropic but complains of halos at night. In the presence of increased amounts of positive spherical aberration and coma, the magnitude of the coefficients of the first- and second-degree modes is different between the Zernike and LDHD decompositions. The sign of the defocus term is positive in the Zernike mode ($z_2^0 = 2.56$ μm, which suggests the presence of a myopic defocus) and one magnitude order lower in the LDHD mode ($g_2^0 = -0.274$ μm). The coefficients of the tilt modes are negligible in the LDHD decomposition, whereas their values in the Zernike decomposition are due to the necessity to compensate for the r^1 terms present in the Zernike coma modes.

The vectorial representations in Fig. 12 underline the differences between the magnitude of the low- and high-wavefront components of f^* in the Zernike versus LDHD decompositions. The magnitude of f_l^* is much lower than that of $f_{z\ell}^*$. The proximity of f_h^* and f^* suggests that the global wavefront error is mostly due to higher-order aberrations. The predominance of fourth-order aberration modes in the wavefront error is better rendered in the new HD expansion.

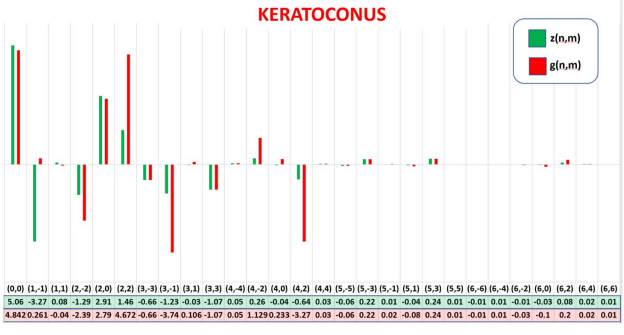

Fig. 9. Comparison between the Zernike and new expansion coefficients of an eye with keratoconus.

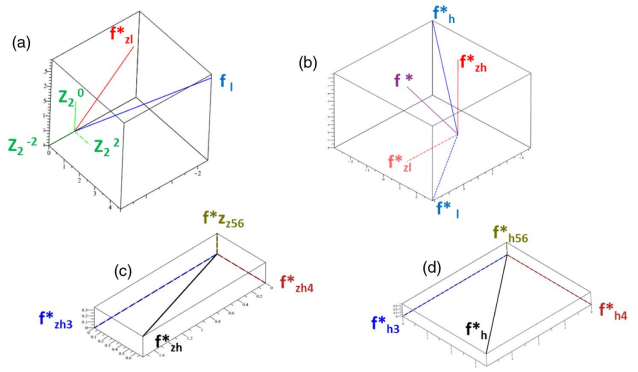

Fig. 10. Geometrical representations of the Zernike and GM expansions: (a) comparison of $f_{z\ell}^*$ and f_ℓ^*; (b) comparison of the Zernike versus LDHD split between low ($f_{z\ell}^*$ versus f_ℓ^*) and high (f_{zh}^* and f_h^*) components; (c),(d) comparison between the Zernike HD versus new HD expansion.

Fig. 11. Comparison between the Zernike and new expansion coefficients of an eye corrected with LASIK for myopia.

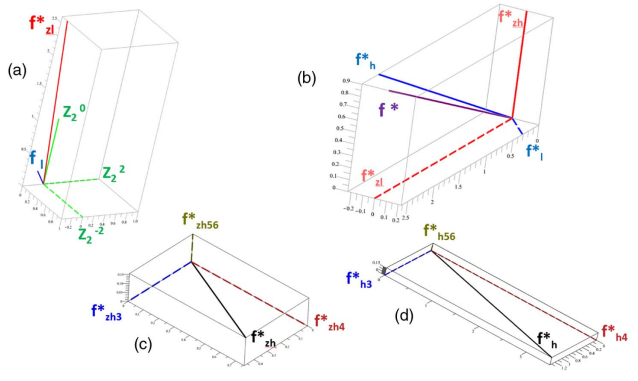

Fig. 12. Geometrical representations of the Zernike and GM expansions: (a) comparison of $f_{z\ell}^*$ and f_ℓ^*; (b) comparison of the Zernike versus LDHD split between low ($f_{z\ell}^*$ versus f_ℓ^*) and high (f_{zh}^* and f_{zh}^*) components; (c),(d) comparison between the Zernike HD versus new HD expansion.

D. Eye with LASIK Performed with Aspheric Photoablation for Hyperopia and Presbyopia

This eye had LASIK performed for combined hyperopia and presbyopia with an aspheric ablation. There is a marked difference between the value of the defocus ($z_2^0 = 0.18$ μm, $g_2^0 = 4.05$ μm) between the two decompositions (Fig. 13). In this case, most of the defocus terms are embedded in the Z_4^0 mode, which is weighted by $z_4^0 = -0.62$ μm. In the LDHD decomposition, the terms in r^2 are decoupled from the terms in r^4.

The spatial representation of the low- and high-order wavefront components obtained through the Zernike and LDHD polynomial basis displays these differences (Fig. 14). The apparent magnitude of each of the main Zernike wavefront components is significantly reduced, compared to the magnitude of their LDHD counterparts. The Zernike HD expansion does not reflect the dominance of the fourth-order aberration modes coefficients (f^*_{zh4}) within the higher-order wavefront component as well as the new HD expansion in which the f^*_{h4} component predominates.

Fig. 13. Comparison between the Zernike and new expansion coefficients of an eye operated with an aspheric photoablation for hyperopia and presbyopia—PresbyLASIK.

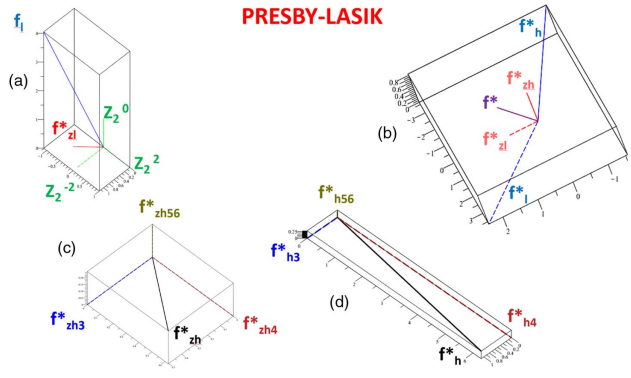

Fig. 14. Spatial representations of the Zernike and LDHD expansion: (a) comparison of $f^*_{z\ell}$ and f^*_{ℓ}; (b) comparison of the Zernike versus LDHD split between low ($f^*_{z\ell}$ versus $f^*_{z\ell}$) and high (f^*_{zh} and f^*_{h}) components; (c),(d) comparison between the Zernike HD versus new HD expansion.

6. DISCUSSION

Wavefront aberrometry is a modern method to measure the optical characteristics of normal and clinically abnormal eyes. It expanded the scope of ocular optics far beyond measuring sphero-cylindrical errors, to include additional optical flaws such as trefoil, coma, and spherical aberration [7,8]. As aberrometers moved from laboratory to the clinic in 2000, a consensus was reached to mathematically describe the complex aberration structure of human eyes in the form of fundamental elements and expressing their respective importance into Zernike coefficients [1]. This consensus led to national (ANSI Z80.28) and international (ISO 24157) standards for reporting the ocular aberrations in a clear and meaningful way. The second-order terms, whose leading component is of order 2 and the other lower-order terms (piston and tilt) are the aberrations traditionally dealt with in ophthalmic optics. Terms of order 3 and higher are therefore referred to as higher-order terms. However, the use of Zernike modes has some drawbacks with regards to the interpretation of the values of the coefficients. As shown in Figs. 3 and 5, in the presence of a theoretical high-order wavefront component free of terms of lower degree than 3, the Zernike expansion brings non-null RMS coefficients for the low-degree Zernike modes to compensate for the r^0, r^1, and r^2 terms which are embedded into the higher-order modes. Since all the odd Zernike high-order modes ($Z_n^{\pm 1}$, $n >= 3$) contain linear terms, the interpretation of the altered Zernike tilt coefficient should not be related to any prismatic deviation of the wavefront. The tilt coefficients of the Zernike series do not bring direct relevant information about any misalignment between the eye and wavefront sensing instrument axes. Because of similar mathematical reasons, the presence of terms of second degree in higher-order Zernike modes with $m < 3$ may alter the interpretation of the z_2^0 coefficient value. The influence of higher-order modes coefficients on the low-order defocus coefficient can be dramatic (Cases 3 and 4).

The decomposition of the wavefront in our new basis requires new coefficients which are obtainable from Zernike expansion after collection of low-order terms. The normalization coefficients of the Zernike modes have higher magnitudes than their corresponding LDHD modes. This results in the minimization of the magnitude of some coefficients of clinical importance, such as $z_3^{\pm 1}$, z_4^0, $z_4^{\pm 2}$, in the Zernike classification as compared to the LDHD classification. This may reduce the apparent contribution of the higher-order wavefront terms in the total wavefront expansion. As the reduction incurred for the fourth-order modes is greater than for the third-order modes, this may also affect the clinical interpretation of the higher-order component, and artificially reduce the apparent contribution of the fourth-order modes to the wavefront error.

Our new mathematical functions do not incur these drawbacks, but keep most of the desirable properties of the Zernike basis. The collection of all the lower terms (r^0, r^1, and r^2) should provide a more pertinent characterization of the low component of the ocular wavefront, equivalent to what would be obtained through a Seidel decomposition. Classical Seidel aberrations are not orthogonal. Stephenson has proposed an alternative series expansion which combines some desirable

characteristics of the Zernike and Seidel classifications [9]. However, the modes in this series were not orthogonal. There is no orthogonality between the low- and higher-order terms in the LDHD split; however, the LDHD scheme preserves the orthogonality within the low-order (f_ℓ) and higher-order (f_h) components, respectively. The lack of orthogonality between the low- and higher-order components does not allow direct calculation of the total wavefront RMS, but this may not be too detrimental in ophthalmic optics, where it is often intrinsic to proper clinical interpretation to consider low- and higher-order aberrations separately. In this new scheme, the third-order coma and primary spherical aberration modes are equivalent to the classic coma and primary Seidel modes, where the wavefront error only varies with the third and fourth power of the pupil radius, respectively. In both of our clinical examples, the magnitude of the coma ($g_3^{\pm 1}$) and spherical aberration (g_4^0) coefficients was larger than that of their corresponding Zernike modes. They may better reflect their exact contribution within the higher-order aberration component of the wavefront. In our second example (eye with keratoconus), the differences in the Zernike and the new LDHD expansion affect both the low- and higher-order wavefront components. The magnitude of the low-order astigmatism is reduced in the Zernike versus new LDHD expansion ($z_2^2 = 1.46$, $g_2^2 = 4.6$ microns). The coefficients of the tilt modes are almost zeroed in the low-order component. The decomposition of the f_h component into Zernike modes highlights the insufficiency of this classification to properly segregate the true low- versus higher-degree components of the ocular wavefront.

Zero-order (piston), first-order (tilt), and second-order (defocus and astigmatism) modes belong to the low-order aberrations group and are traditionally corrected with the prescription of spectacles or contact lenses. High-order aberrations comprise the third- and higher-order modes of the Zernike classification. The least-square fitting of an aberration map with a quadratic surface leads to the value of second-order Zernike coefficients, which include the second-order aberrations of defocus and astigmatism. These second-order Zernike coefficients can be converted to a sphero-cylindrical prescription in power vector notation [10]. Many studies have shown that the coefficients of low-order aberrations (second-degree Zernike modes) do not enable prediction of subjective refraction accurately [6,11,12]. The Zernike defocus is that which best fits the wavefront aberration in an RMS sense over a particular circular pupil, whereas the full pupil refraction appears to be dominated by near paraxial optics. Several studies have shown that eliminating the second-order Zernike aberrations does not necessarily optimize the subjective impression of best-focus nor the objective measurement of visual performance [10,13,14]. Eliminating second-order Zernike aberrations is equivalent to minimizing the RMS wavefront error, but this minimization does not necessarily optimize the quality of the retinal image [10].

Matching paraxial curvature of the ocular wavefront can accurately predict the results of subjective refraction. This method is closely related to the Seidel expansion of wavefronts because it isolates the purely parabolic (r^2) term. It also corresponds to a paraxial analysis since the r^2 coefficient is zero when the paraxial rays are well focused. This method was accurate to within 1/8D for predicting astigmatism, which may be sufficient for most clinical purposes [10].

In addition, Zernike primary spherical aberration has been experimentally manipulated and it has been shown that its primary effect on the refractive error and image quality is actually caused by the low-order term r^2, which is embedded in this polynomial [6]. Similarly, the level of r^2 embedded in secondary spherical aberration can affect image quality and refraction [15]. Hence, in situations where there is a significant increase in primary and secondary Zernike spherical aberration, the prediction of subjective refraction from the z_2^0 coefficient may be even more inaccurate, as this term will not include the r^2 terms parceled in higher-order modes, such as Z_4^0 and Z_6^0. Our third and fourth clinical examples highlight this situation. In the third clinical example the wavefront error of the eye operated with myopic LASIK is predominantly in r^4 across the pupil, but the Zernike fitting of it results in an increase in the magnitudes of both the z_4^0 and z_6^0 coefficients. This suggests the presence of a strong defocus component in an otherwise post-refractive surgery emmetropic eye. The discrepancy between the low-order coefficients can be explained by the presence of high levels of positive spherical aberration. The value of the z_2^0 coefficient would suggest the presence of a myopic refraction; however, the r^2 terms comprised in that mode are induced in the wavefront decomposition to cancel the r^2 terms embedded in the Z_4^0 mode. Similar compensation occurs for the r^1 terms comprised in the tilt coefficients ($z_1^{\pm 1}$) and the coma coefficients ($z_3^{\pm 1}$). The fourth clinical example corresponds to a situation where most of the quadratic error of the wavefront is "hidden" in the Z_4^0 mode. However, this quadratic wavefront error accounts for the myopic refraction, which is unveiled in the new LDHD expansion.

Because its higher-order modes are devoid of quadratic terms, our new basis can be used to better fit the higher-order component of the wavefront (which should not be contaminated by r^2 terms). In addition, the collection of the quadratic defocus terms to obtain (g_2^0, $g_2^{\pm 2}$) should better predict the objective refraction of a given eye, and the remaining error could then be decomposed into the new HD basis without inducing quadratic terms. The application of wavefront analysis technology to the human eye has allowed refractive surgeons to identify and treat HOAs, in addition to sphere and cylinder. This has led to potentially significant improvement in the quality of vision following refractive surgery and the ability to correct preexisting or induced post-surgical HOAs. Since it provides a clearer separation between the low- and higher-order wavefront components, our method reduces the risk of miscalculations in procedure planning inherent to the presence of low-order terms in higher-order Zernike modes. This method should also provide better accuracy for predicting the retinal image quality from pupil-based quality metrics related to the best spectacle correction [16] and a better understanding of the selective impact of higher-order terms on the depth of focus [17–20].

REFERENCES

1. L. Thibos, R. Applegate, J. Schwiegerling, and R. Webb, and VSIA Standards Taskforce Members: Vision Science and Its Applications, "Standards for reporting the optical aberrations of eyes," J. Refractive Surg. **18**, S652–S660 (2002).

2. V. Mahajan, "Zernike circle polynomials and optical aberrations of systems with circular pupils," Appl. Opt. **33**, 8121–8124 (1994).
3. F. Zernike, "Beugungstheorie des schneidenverfahrens und seiner verbesserten form, der phasenkontrastmethode," Physica **1**, 689–704 (1934).
4. R. Noll, "Zernike polynomials and atmospheric turbulence," J. Opt. Soc. Am. **66**, 207–211 (1976).
5. A. Bradley, R. Xu, L. Thibos, G. Marin, and M. Hernandez, "Influence of spherical aberration, stimulus spatial frequency, and pupil apodisation on subjective refractions," Ophthalmic Physiolog. Opt. **34**, 309–320 (2014).
6. X. Cheng, A. Bradley, S. Ravimukar, and L. Thibos, "Visual impact of Zernike and Seidel forms of monochromatic aberrations," Optom. Vis. Sci. **87**, 300–312 (2010).
7. M. Smirnov, "Measurement of the wave aberration of the human eye," Biophysics **24**, 766–795 (1961).
8. J. Liang, B. Grimme, S. Goelz, and J. Bille, "Objective measurement of the wave aberration of the human eye using a Shack-Hartmann wavefront sensor," J. Opt. Soc. Am. **11**, 1949–1957 (1994).
9. P. Stephenson, "Optical aberrations described by an alternative series expansion," J. Opt. Soc. Am. **26**, 265–273 (2009).
10. L. Thibos, X. Hong, A. Bradley, and R. Applegate, "Accuracy and precision of objective refraction from wavefront aberrations," J. Vis. **4** (4):9, 329–351 (2004).
11. X. Cheng, A. Bradley, and L. Thibos, "Predicting subjective judgment of best focus with objective image quality metrics," J. Vis. **4**(4):7, 310–321 (2004).
12. L. Chen, B. Singer, A. Guirao, J. Porter, and D. Williams, "Image metrics for predicting subjective image quality," Optom. Vis. Sci. **82**, 358–369 (2005).
13. R. Applegate, C. Ballentine, B. Gross, E. Sarver, and C. Sarver, "Visual acuity as a function of Zernike mode and level of root mean square error," Optom. Vis. Sci. **80**, 97–105 (2003).
14. A. Guirao and D. Williams, "A method to predict refractive errors from wave aberration data," Optom. Vis. Sci. **80**, 36–42 (2003).
15. R. Xu, A. Bradley, N. L. Gil, and L. Thibos, "Modelling the effects of secondary spherical aberration on refractive error, image quality and depth of focus," Ophthalmic Physiolog. Opt. **35**, 28–38 (2015).
16. A. Guirao, J. Porter, D. Williams, and I. Cox, "Calculated impact of higher-order monochromatic aberrations on retinal image quality in a population of human eyes," J. Opt. Soc. Am. A **19**, 1–9 (2002).
17. F. Yi, D. Iskander, and M. Collins, "Depth of focus and visual acuity with primary and secondary spherical aberration," Vis. Res. **51**, 1648–1658 (2011).
18. R. Legras, Y. Benard, and N. Lopez-Gil, "Effect of coma and spherical aberration on depth-of-focus measured using adaptive optics and computationally blurred images," J. Cataract. Refract. Surg. **38**, 458–469 (2012).
19. L. Zheleznyak, R. Sabesan, J. Oh, S. MacRae, and G. Yoon, "Modified monovision with spherical aberration to improve presbyopic through-focus visual performance," Invest. Ophthalmol. Vis. Sci. **54**, 3157–3165 (2013).
20. L. Zheleznyak, H. Jung, and G. Yoon, "Impact of pupil transmission apodization on presbyopic through-focus visual performance with spherical aberration," Invest. Ophthalmol. Vis. Sci. **55**, 70–77 (2014).